minerals

MDPI

Article

Effect of Different Mineralogical Proportions on the Electrical Conductivity of Dry Hot-Pressed Sintering Gabbro at High Temperatures and Pressures

Mengqi Wang [1,2], Lidong Dai [1,*], Haiying Hu [1,*], Wenqing Sun [1], Ziming Hu [1,2] and Chenxin Jing [1,2]

[1] Key Laboratory of High-Temperature and High-Pressure Study of the Earth's Interior, Institute of Geochemistry, Chinese Academy of Sciences, Guiyang 550081, China; wangmengqi@vip.gyig.ac.cn (M.W.); sunwenqing@vip.gyig.ac.cn (W.S.); huziming@mail.gyig.ac.cn (Z.H.); jingchenxin@mail.gyig.ac.cn (C.J.)
[2] University of Chinese Academy of Sciences, Beijing 100049, China
* Correspondence: dailidong@vip.gyig.ac.cn (L.D.); huhaiying@vip.gyig.ac.cn (H.H.)

Abstract: Electrical conductivities of the dry hot-pressed sintering gabbro with various mineralogical proportions (Cpx_XPl_{100-X}, X = 0, 10, 20, 30, 40, 50, 60, 70, 80, 90 and 100 vol% (the signals of Cpx and Pl denote clinopyroxene and plagioclase, respectively) were measured in the YJ-3000t multi-anvil pressure and Solartron-1260 impedance spectroscopy analyzer at temperatures of 773–1073 K and pressures of 1.0–3.0 GPa. At the given pressure conditions, the electrical conductivity and temperature conformed to an Arrhenius relation. For the fixed mineralogical composition of $Cpx_{50}Pl_{50}$, the electrical conductivities of the samples significantly increased with the rise of temperature, but slightly decreased with increasing pressure. Furthermore, the activation energy and activation volume were determined as 1.06 ± 0.12 eV and 6.00 ± 2.00 cm^3/mole, respectively. As for the various mineralogical compositions of dry gabbro, the electrical conductivities of the samples increased with the rise of volume percentage of clinopyroxene (*Cpx*) at 1.0 GPa. It is proposed that the main conduction mechanism is the small polaron, owing to the positive relation between the electrical conductivity and the iron content in samples. On the basis of these obtained conductivity results, laboratory-based electrical conductivity–depth profiles for the hot-pressed sintering gabbro with various mineralogical proportions and temperature gradients were successfully established. In conclusion, although the present acquired electrical conductivity results on the dry hot-pressed sintering gabbro with various mineralogical proportions cannot explain the high conductivity anomaly in the oceanic crust and West African craton, it can provide one reasonable constraint on the mineralogical composition in these representative gabbro-rich regions.

Keywords: electrical conductivity; gabbro; mineralogical proportions; high temperature; high pressure

Citation: Wang, M.; Dai, L.; Hu, H.; Sun, W.; Hu, Z.; Jing, C. Effect of Different Mineralogical Proportions on the Electrical Conductivity of Dry Hot-Pressed Sintering Gabbro at High Temperatures and Pressures. *Minerals* **2022**, *12*, 336. https://doi.org/10.3390/min12030336

Academic Editor: Julien Siebert

Received: 8 February 2022
Accepted: 4 March 2022
Published: 8 March 2022

1. Introduction

Results of the field geophysical observations from magnetotelluric (MT) and geomagnetic deep sounding (GDS) have confirmed that there is widespread existence of a large quantity of the anomalously high electrical conductivity phenomena in these typical regions of oceanic crust [1–3] and West African craton [4]. As a representative basic intrusive rock, it is well known that gabbro is widely outcropped in these global tectonic units of oceanic crust and craton regions, and its corresponding dominant mineralogical composition is constituted of clinopyroxene and plagioclase [5,6]. Therefore, a systematic investigation of the electrical conductivity of gabbro at high temperature and high pressure is crucial to deeply explore the cause of high conductivity anomaly in these regions.

As for natural gabbro, there are a large quantity of previously available reported electrical conductivity results using the piston-cylinder and multi-anvil press at conditions of high temperature and high pressure [7–10]. Wang et al. [7] measured the electrical conductivities of dry natural gabbro at pressures of 1.0–2.0 GPa and temperatures of

593–1173 K and found that the electrical conductivity significantly decreased by two orders of magnitude with the rise of pressure. The electrical conductivity and P-wave elastic velocity for natural biotite-bearing gabbro were determined by Bai et al. [8] within the temperature ranges from 293 K to 1373 K and pressure ranges from 1.0 GPa to 2.0 GPa. They proposed that the dehydration reaction of the accessory of hydrous biotite occurred at the critical temperature ranges of 1073–1123 K, and thus resulted in the appearance of the partial melting. Dai et al. [9] conducted electrical conductivity on the natural hydrous gabbro at conditions of 623–1173 K and 0.5–2.0 GPa, and three different solid oxygen buffers to control the oxygen fugacity (e.g., Cu + CuO, Ni + NiO, and Mo + MoO_2). Their mineralogical compositions of natural gabbro were composed of 60% plagioclase, 39% augite, and ~1% minor mineral phases. Some hydrogen-related defects in the natural hydrous gabbro with the relatively lower concentration were considered as the main charge carrier because a negative dependence relationship between the electrical conductivity and oxygen fugacity was observed by Dai et al. [9]. More recently, Saito and Bagdassarov [10] performed laboratory measurements of the electrical conductivity for gabbro samples in the Oman ophiolite at 523–1181 K and 0.6–0.8 GPa using the piston-cylinder high-pressure apparatus. In comprehensive considerations of all previously acquired conductivity results, we find that there exists one obvious discrepancy of almost three magnitude orders in the electrical conductivity of natural gabbro, which possibly originates from the differentiation of mineralogical proportion, water content, and accessory minerals.

As usual, the laboratory-based electrical conductivity of rock is highly correlated with its main constituent minerals at high temperate and high pressure. As two dominant constituent minerals in gabbro, electrical conductivities of clinopyroxene and plagioclase single crystals have been studied extensively. Yang et al. [11] obtained the electrical conductivities of lower crustal clinopyroxene at temperatures of 523–1273 K and pressures of 0.6–1.2 GPa in a piston-cylinder press. Electrical conductivities of anhydrous and hydrous clinopyroxene were measured by Zhao and Yoshino [12] at temperatures of 600–1200 K and 1.5 GPa in a DIA-type multi-anvil apparatus. By virtue of the Wayne Kerr B642 alternating current analyzer at a fixed frequency of 1.6 kHz, electrical conductivities of natural and synthetic polycrystalline diopside were measured at temperatures of 913–1337 K and pressure of 1.0 GPa [13]. Liu et al. [14] carried out the impedance spectroscopic measurements on omphacite single crystals containing 7.92 wt% iron and 0.0085 wt% water at temperatures of 623–973 K and 1.0 GPa in a piston-cylinder press. Sun et al. [15] researched the electrical conductivities of the clinopyroxene–NaCl–H_2O systems with various fluid fractions and salinities at 673–973 K and 1.0 GPa, and they found that the NaCl-bearing aqueous fluids in clinopyroxene can greatly enhance the electrical conductivity of fluid-bearing sample. Except for these abovementioned electrical conductivity results on clinopyroxene, Yang et al. [16] also performed the measurement of the electrical conductivity of lower crustal plagioclase (its corresponding chemical composition is $An_{66}Ab_{32}Or_2$. Here, *An*, *Ab*, and *Or* denote anorthite, albite, and orthoclase, respectively) at temperatures of 573–1273 K and pressures of 0.6–1.2 GPa, and further, the correlation between the electrical conductivity of plagioclase and water content was successfully established. It is well known that plagioclase is regarded as the solid solution of albite and anorthite. To explore the electrical transport mechanism for the feldspar family, Hu et al. [17,18] measured electrical conductivities of albite and anorthite within the temperature ranges from 773 K to 1073 K and pressure ranges from 1.0 GPa to 3.0 GPa in a YJ-3000t multi-anvil press. They found that the dominant conduction mechanisms for albite and anorthite are of the alkali ion, i.e., the monovalent cationic sodium and bivalent cationic calcium, respectively.

Because of the existence of heterogeneity in the mineralogical compositions and its corresponding mineralogical proportion between the clinopyroxene and plagioclase in different gabbro samples, it is impossible to directly extrapolate the electrical conductivity of gabbro from its main constituent minerals. Therefore, it is crucial to make a systematic study of electrical conductivity for gabbro with different mineralogical proportions at certain mineralogical compositions at high temperature and high pressure.

In the present study, we researched the electrical conductivities of dry hot-pressed sintering gabbro with various mineralogical proportions (Cpx_XPl_{100-X}, X = 0, 10, 20, 30, 40, 50, 60, 70, 80, 90 and 100 vol% at temperatures of 773–1073 K and pressures of 1.0–3.0 GPa. Further, the functional relationship between the electrical conductivity of sample and influential factors (e.g., temperature, pressure, and mineralogical proportion) was deeply explored. Based on these obtained electrical conductivity results and various thermodynamic parameters, we constructed the laboratory-based electrical conductivity–depth profile. Finally, the anomalously high electrical conductivity phenomena in oceanic crust and West African craton are discussed in detail.

2. Experimental Procedures

2.1. Sample Preparation

The natural gem-grade clinopyroxene (*Cpx*) and plagioclase (*Pl*) single crystals were chosen as the starting materials in order to synthesize the gabbro. The results of chemical composition of the main constituent minerals in the hot-pressed sintering gabbro was analyzed by virtue of the electron microprobe, as shown in Table 1.

Table 1. The chemical composition of the main constituent minerals in the hot-pressed sintering gabbro by virtue of the electron microprobe analysis.

Oxides (wt%)	Clinopyroxene (*Cpx*)	Plagioclase (*Pl*)
SiO_2	53.90	52.94
TiO_2	0.13	0.03
Al_2O_3	0.25	26.72
FeO	1.62	0.85
MnO	0.06	0.01
MgO	17.90	0.03
CaO	24.71	13.22
Na_2O	0.22	5.39
K_2O	0.00	0.06
NiO	0.02	0.00
Cr_2O_3	0.23	0.00
Total	99.04	99.25

The *Cpx* and *Pl* single crystal grains were cleaned in a mixture of distilled water, acetone, and ethanol, and then crushed and ground to powders with the grain size of 25 μm. Then, the mineral powders were homogeneously mixed with various volume percentages (Cpx_xPl_{100-x}, X = 0, 10, 20, 30, 40, 50, 60, 70, 80, 90 and 100 vol%) in the agate mortar and loaded into a copper–nickel doubly encapsulated sample chamber. The copper tube has a diameter of 8.5 mm, a thickness of 0.5 mm, and a height of 18.0 mm. To avoid interdiffusion between the copper tube and sample powder, 0.025 mm of nickel foil was adopted to encapsulate it. Subsequently, the sample assemblage was installed in the YJ-3000t multi-anvil high-pressure apparatus in order to complete the hot-pressed sintering of each gabbro with various mineralogical proportions. At the constant pressure of 1.0 GPa, the temperature in the sample chamber was 1073 K for 4 h. After that, the recovered samples were cut and polished into cylinders with diameters of 6.0 mm and heights of 4.0 mm. Lastly, the hot-pressed sintering gabbro was kept in the vacuum dry furnace at 423 K for at least 12 h before the in situ electrical conductivity measurements.

To identify the distribution of the minerals in hot-pressed sintering gabbro samples, four representative backscattered electron images of dry hot-pressed sintering gabbro with various mineralogical proportions were observed by using scanning electron microscope, as displayed in detail in Figure 1. As a whole, the distributions of *Cpx* and *Pl* grains in the acquired synthetic gabbro are almost homogeneous, and the magnitude of grain size is ~25 μm. As pointed out by Yang and Heidelbach [19], when the grain size of hot-pressed sintering synthetic clinopyroxene is larger than 10 μm, the influence of grain size on the electrical conductivity of a sample can be negligible under conditions of similar temperature

and pressure ranges. Thus, the effect of grain size on the electrical conductivity of synthetic gabbro did not need to be considered in this study.

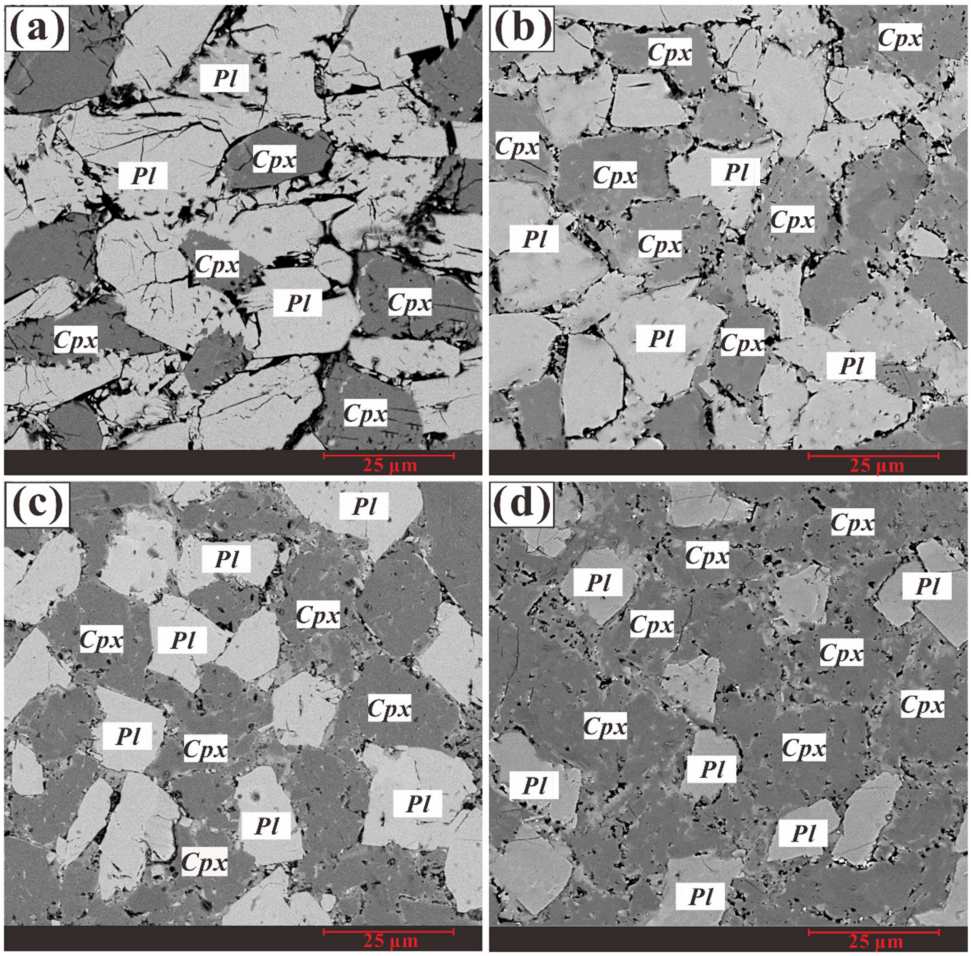

Figure 1. Four representative backscattered electron images of dry hot-pressed sintering gabbro by using scanning electron microscope with different mineralogical proportions: (**a**) $Cpx_{20}Pl_{80}$, (**b**) $Cpx_{40}Pl_{60}$, (**c**) $Cpx_{60}Pl_{40}$, and (**d**) $Cpx_{80}Pl_{20}$. *Cpx* and *Pl* represent clinopyroxene and plagioclase, respectively.

To accurately determine the water contents in the hot-pressed sintering gabbro before and after electrical conductivity experiments, the infrared spectra of samples were measured for each individual constituent *Cpx* and *Pl* mineral phases by a Fourier transform infrared spectrometer (Vertex-70V and Hyperion-1000 infrared microscope). The samples for Fourier transform infrared spectroscopy analysis (FT-IR) were double-polished up to a thickness of less than 200 μm. As shown in Figure 2, the FT-IR absorption spectra for clinopyroxene and plagioclase were conducted within the wavenumber range of 3000–4000 cm^{-1} in the hot-pressed sintering gabbro, respectively. By virtue of the representative hydrogen-related bands within the range of 3000–3750 cm^{-1}, the water content in the sample was calculated by the modified equation of the Beer–Lambert law [20]. The obtained water content in the sample is less than 25 ppm wt, which is almost anhydrous. A detailed description for the FT-IR measurement was given in the previous reference [21].

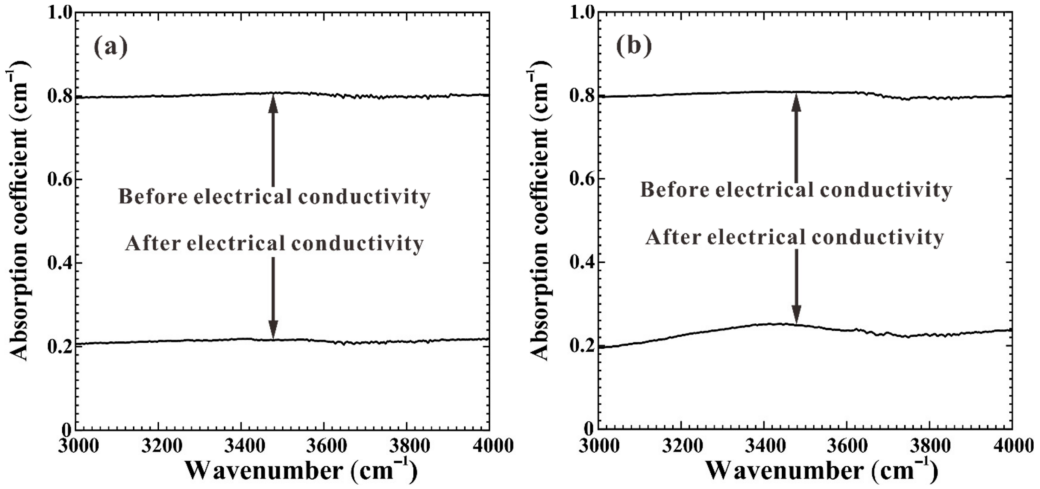

Figure 2. FT-IR spectra in the dry hot-pressed sintering gabbro before and after electrical conductivity measurements within the wavenumber range of 3000–4000 cm^{-1}. Here, (**a**,**b**) represent the clinopyroxene and plagioclase in the dry hot-pressed sintering gabbro, respectively.

2.2. High-Pressure Cell and Impedance Measurements

Electrical conductivity measurements were performed with the YJ-3000t multi-anvil apparatus and a Solartron-1260 Impedance/Gain-phase analyzer. Detailed measurement principles and experimental procedures are described by Dai et al. [22] and Hu et al. [23]. Figure 3 shows the schematic diagram of the experimental assemblage for electrical conductivity measurements at high pressure and temperature. Pyrophyllite with edge length of 32.5 mm was used as the pressure medium. The heater with a thickness of 0.5 mm consisted of three-layer stainless-steel sheets. The alumina and magnesia sleeves were adopted to provide a good insulation environment. The nickel foil (thickness: 0.025 mm) between the insulation sleeves was installed, which was directly linked to the Earth line to shield against the spurious signal interference and external electromagnetism. All these parts were baked at 1073 K for 5 h in a muffle furnace before the electrical conductivity of sample assembly. Two symmetric nickel disks with thickness of 0.5 mm and correspondent diameter of 6.0 mm were installed at both ends of the sample as measurement electrodes. A K-type thermocouple was used to monitor the temperature during the process of electrical conductivity measurements at high pressure.

For each electrical conductivity measurement, pressure was enhanced with a rate of 1.0 GPa/h to the desired value. Under the constant pressure condition, the temperature was gradually increased with a speed of 120 K/h. At a given temperature and pressure, the impedance spectra of samples were measured on the Solartron-1260 Impedance/Gain-phase analyzer with an applied voltage of 1.0 V signal voltage within the frequency range of 10^{-1}–10^{6} Hz. To check the reproducibility of electrical conductivity result, each electrical conductivity measurement in the sample was continuously measured at least two heating and cooling cycles. The uncertainties from the experimental pressure and temperature were less than 0.1 GPa and 5 K, respectively.

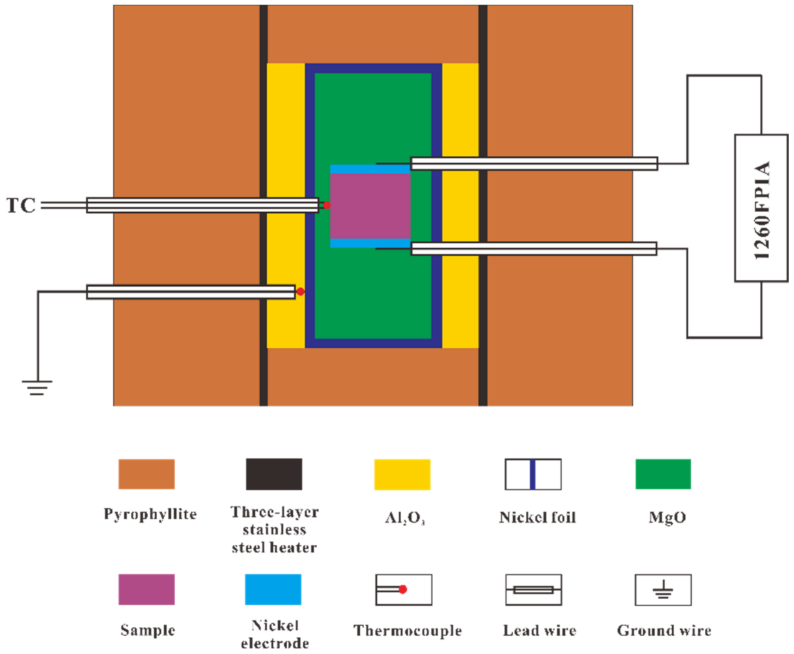

Figure 3. The experimental setup for electrical conductivity measurements at high temperature and high pressure.

3. Results

In the experiments, we measured the electrical conductivities of dry gabbro with various mineralogical proportions (Cpx_xPl_{100-x}, X = 0, 10, 20, 30, 40, 50, 60, 70, 80, 90 and 100 vol%) at temperature ranges of 773–1073 K and 1.0 GPa. To explore the effect of pressure on the conductivity of the dry gabbro, the electrical conductivities of $Cpx_{50}Pl_{50}$ sample were measured at temperature ranges of 773–1073 K and pressure ranges of 1.0–3.0 GPa.

Typical complex impedance spectra of hot-pressed sintering gabbro ($Cpx_{50}Pl_{50}$) at temperature ranges of 773–1073 K and pressure of 1.0 GPa are shown in Figure 4. The impedance spectra arcs were composed of an ideal semicircular arc within the high-frequency range from 10^6 Hz to ~1 Hz and another extra small tail at the frequency range from ~1 Hz to 10^{-1} Hz, which reflected the electrical transport process of grain interior and polarization effect at the sample–electrode interface, respectively [24]. Therefore, the equivalent circuit composed of the series connection of R_S-CPE_S (R_S and CPE_S represent the resistance and the constant phase element from the grain interior, respectively) and R_E-CPE_E (R_E and CPE_E represent the resistance and the constant phase element from the polarization effect at the sample–electrode interface, respectively) were adopted to fit the impedance spectra arc and acquire the conductivity results.

The electrical conductivities of the samples were calculated by the following equation,

$$\sigma = L / SR \quad (1)$$

where σ is the electrical conductivity of the sample (S/m), R is the resistance (Ω), L is the length of the sample (m), and S is the cross-sectional area of the electrode (m^2). The electrical conductivities of the hot-pressed sintering gabbro and the temperatures conformed to the Arrhenius relation,

$$\sigma = \sigma_0 \exp(-\Delta H / kT) \quad (2)$$

where σ_0 is the pre-exponential factor (S/m), k is the Boltzmann constant, T is the absolute temperature (K), and ΔH is the activation enthalpy (eV). The fitting parameters for the electrical conductivities are listed in Table 2.

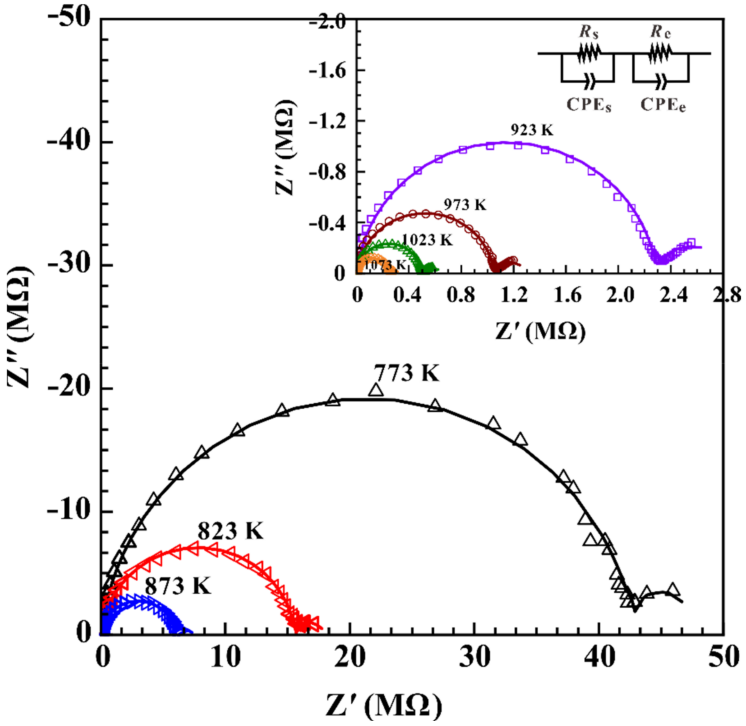

Figure 4. Typical complex impedance spectra for the $Cpx_{50}Pl_{50}$ sample, obtained at temperatures of 773–1073 K and pressure of 1.0 GPa in the frequency range from 10^{-1} Hz to 10^{6} Hz. Z' and Z'' are the real and imaginary parts of the complex impedance, respectively. The equivalent circuit that is composed of the series connection of R_S-CPE_S and R_E-CPE_E (R_S and CPE_S represent the resistance and the constant-phase element of the bulk impedance for the sample, respectively; R_E and CPE_E represent the resistance and the constant phase element from the polarization effect of the sample-electrode interface, respectively) is selected to model the impedance semicircles. The fitting results for the experimental data are displayed by using the solid line.

Table 2. Fitted parameters of the Arrhenius relation for the electrical conductivity of dry hot-pressed sintering gabbro samples. P is pressure, T is temperature, σ_0 is the pre-exponential factor, ΔH is activation enthalpy, and R^2 is the linear correction.

Run No.	Sample	P (GPa)	T (K)	Log [σ_0 (S/m)]	ΔH (eV)	R^2
DW02	Dry *Pl*	1	773–1073	2.43 ± 0.16	1.28 ± 0.03	99.68
DW04	$Cpx_{10}Pl_{90}$	1	773–1073	2.36 ± 0.07	1.26 ± 0.01	99.94
DW06	$Cpx_{20}Pl_{80}$	1	773–1073	2.36 ± 0.09	1.25 ± 0.02	99.90
DW08	$Cpx_{30}Pl_{70}$	1	773–1073	2.38 ± 0.12	1.24 ± 0.02	99.81
DW10	$Cpx_{40}Pl_{60}$	1	773–1073	2.40 ± 0.07	1.23 ± 0.01	99.93
DW12	$Cpx_{50}Pl_{50}$	1	773–1073	2.46 ± 0.06	1.23 ± 0.01	99.91
DW26	$Cpx_{50}Pl_{50}$	2	773–1073	2.77 ± 0.21	1.32 ± 0.04	99.52
DW28	$Cpx_{50}Pl_{50}$	3	773–1073	2.88 ± 0.23	1.37 ± 0.05	99.33
DW14	$Cpx_{60}Pl_{40}$	1	773–1073	2.52 ± 0.08	1.23 ± 0.01	99.78
DW16	$Cpx_{70}Pl_{30}$	1	773–1073	2.56 ± 0.11	1.22 ± 0.01	99.96
DW18	$Cpx_{80}Pl_{20}$	1	773–1073	2.53 ± 0.06	1.21 ± 0.01	99.95
DW20	$Cpx_{90}Pl_{10}$	1	773–1073	2.31 ± 0.07	1.15 ± 0.01	99.93
DW22	Dry *Cpx*	1	773–1073	2.02 ± 0.01	1.09 ± 0.01	99.95

For two fixed mineralogical proportions of $Cpx_{30}Pl_{70}$ and $Cpx_{70}Pl_{30}$ gabbro, the electrical conductivities of samples among two heating–cooling cycles at a pressure of 1.0 GPa are shown in Figure 5, respectively. In the first heating process, it is clear that a relatively higher value of electrical conductivity in gabbro was observed, which is possibly owing to the disequilibrium of thermal transference at 1.0 GPa. Subsequently, the electrical conductivity of the sample is almost reproducible in the first cooling and another heating–cooling cycle.

A good reproducibility in the electrical conductivity of sample denotes a completely stable and equivalent state to be reached in the sample chamber during the process of electrical conductivity measurement, which will be also adopted to fit the following electrical conductivity results.

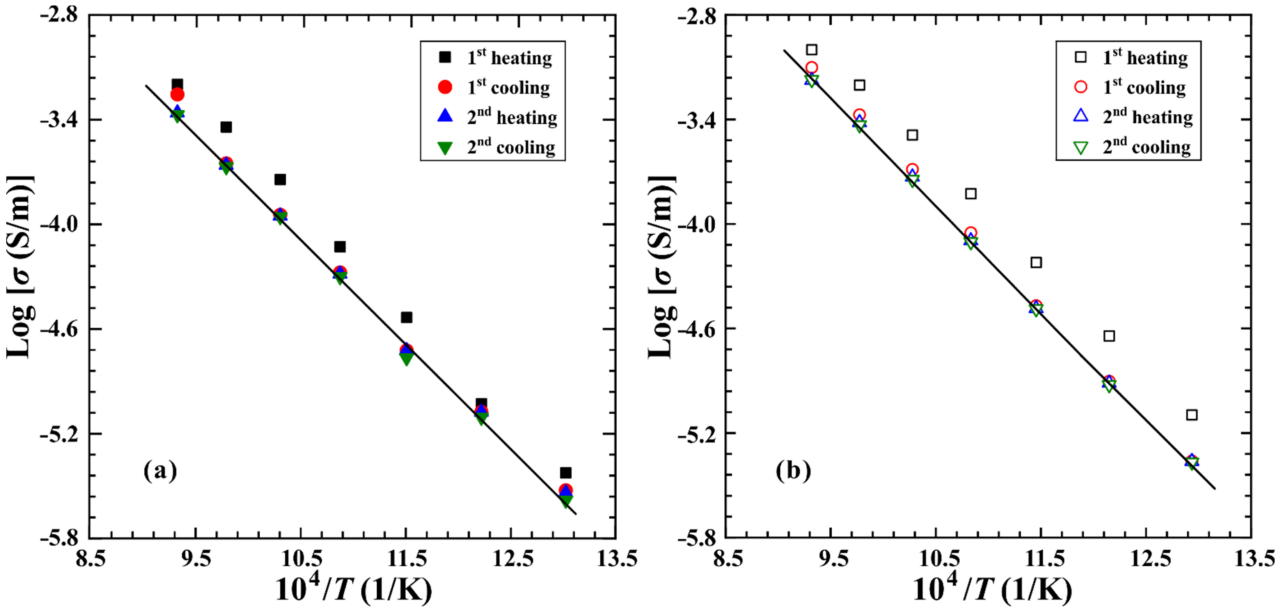

Figure 5. The electrical conductivities of the hot-pressed sintering gabbro among two heating–cooling cycles at a pressure of 1.0 GPa. Here, (**a**,**b**) represent the samples of $Cpx_{30}Pl_{70}$ and $Cpx_{70}Pl_{30}$, respectively.

4. Discussions

4.1. Influence of Pressure on Electrical Conductivity

To identify the effect of pressure on the electrical conductivity of gabbro, we measured the electrical conductivities of dry hot-pressed sintering gabbro ($Cpx_{50}Pl_{50}$) at pressures of 1.0–3.0 GPa. As shown in Figure 6, the electrical conductivity of the sample slightly decreases with the rise of pressure at temperature ranges of 773–1073 K. Further, the pre-exponential factor increased from 2.51×10^2 S/m to 7.59×10^2 S/m and activation enthalpy raised from 1.23 eV to 1.35 eV with the rise of 1.0 GPa to 3.0 GPa, respectively. In the present studies, the influence of pressure on the electrical conductivity can be described as

$$\sigma = A_0 \cdot (1 - BP) \cdot \exp\left(\frac{\Delta U + P\Delta V}{kT}\right) \quad (3)$$

Here, the pre-exponential factor (σ_0) and activation enthalpy (ΔH) of pressure dependence can be described as the equations of $\sigma_0 = A_0(1 - BP)$ and $\Delta H = \Delta U + P\Delta V$, where ΔU is the activation energy (eV), ΔV is the activation volume (cm^3/mole), P is pressure (GPa), and B is a constant with a dimension of 1/GPa. Therefore, the globally fitting data was adopted to fit it, and the fitting results are shown in Table 3. The logarithmic electrical conductivity of hot-pressed sintering sample and the inverse temperature follows a good linear relation, which reveals only one conduction mechanism operating the electrical transport within our experimental pressure ranges. By virtue of the Arrhenius relationship between the electrical conductivity and temperature at different pressures, we can extrapolate a linear relationship between log σ and the reciprocal temperature at atmospheric pressure. Furthermore, the pre-exponential factor and activation enthalpy at room pressure are calculated as 1.99×10^2 S/m and 1.17 eV, respectively. According to Equation (3) and Table 3, the activation energy and activation volume of the dry gabbro ($Cpx_{50}Pl_{50}$) can be determined as 1.06 ± 0.12 eV and 6.00 ± 2.00 cm^3/mole.

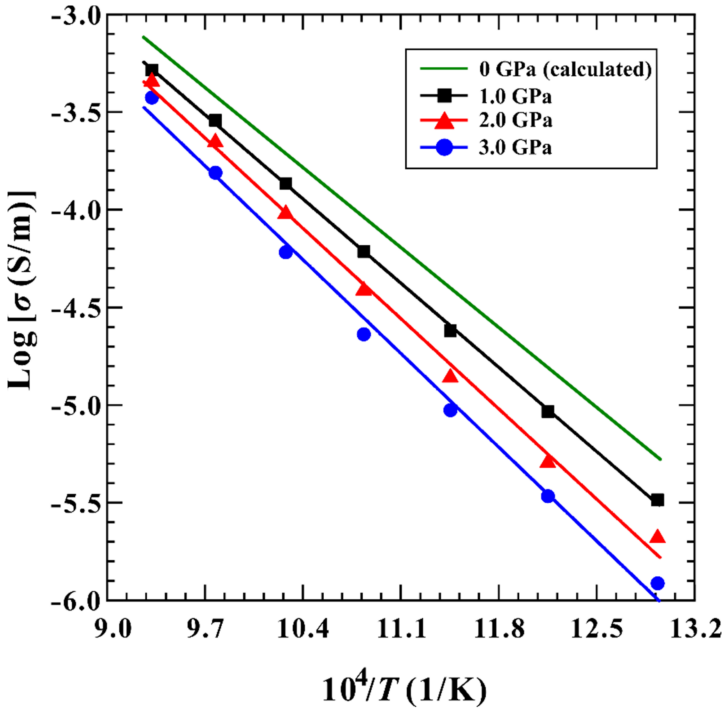

Figure 6. Influence of pressure on the electrical conductivity of dry hot-pressed sintering gabbro ($Cpx_{50}Pl_{50}$) at the temperature ranges of 773–1073 K.

Table 3. Parameter values for the electrical conductivity of dry hot-pressed sintering gabbro $Cpx_{50}Pl_{50}$ (units: σ_0: S/m, ΔU: kJ/mole, ΔV: cm^3/mole, P: GPa). The equation $\sigma = \sigma_0 \exp(\frac{\Delta U + P\Delta V}{kT})$ is adopted for the globally fitting of electrical conductivity data in sample. Considering the strong dependence on experimental data of σ_0 value on pressure, we used the relation $\sigma_0 = A_0(1 - BP)$ (where the unit for B is 1/GPa).

σ_0	ΔU (kJ/Mole)	ΔV (cm^3/Mole)
A_0 = 92.40 ± 14 (S/m) B = 0.23 ± 0.02 (1/GPa)	102 ± 12	6.00 ± 2.00

In the present study, we observed a negative dependence relation for the electrical conductivity of dry hot-pressed sintering gabbro ($Cpx_{50}Pl_{50}$) on the pressure, which is in good consistency with previously reported results [8]. In addition, Dai et al. [9] also investigated the electrical conductivity of natural gabbro at conditions of temperature ranges from 623 K to 1173 K, pressure ranges from 0.5 GPa to 2.0 GPa, and controlled different oxygen fugacities by three solid buffers (Cu + CuO, Ni + NiO, and Mo + MoO_2). On the contrary, a positive dependence relationship between the effect of electrical conductivity of natural gabbro and pressure was observed at a similar experimental condition. It is possibly related to the water content of the gabbro sample, which is also found to have a similar pressure effect to those of previously available electrical conductivity of anhydrous pyrope-rich and almandine-rich garnet single crystals at high temperature and high pressure [9,25,26].

4.2. Influence of Mineralogical Proportions on Electrical Conductivity

We have already measured the electrical conductivity on the hot-pressed sintering gabbro with various mineralogical proportions (Cpx_XPl_{100-X}, X = 0, 10, 20, 30, 40, 50, 60, 70, 80, 90 and 100 vol%) under conditions of 873–1473 K, 1.0 GPa, and the Ni–NiO solid buffer. The chemical composition of gabbro sample is well controlled by changing the mineralogical proportion of clinopyroxene and plagioclase. At a fixed pressure of

1.0 GPa, the effects of mineralogical proportions on the electrical conductivity of gabbro are illustrated in Figures 7 and 8.

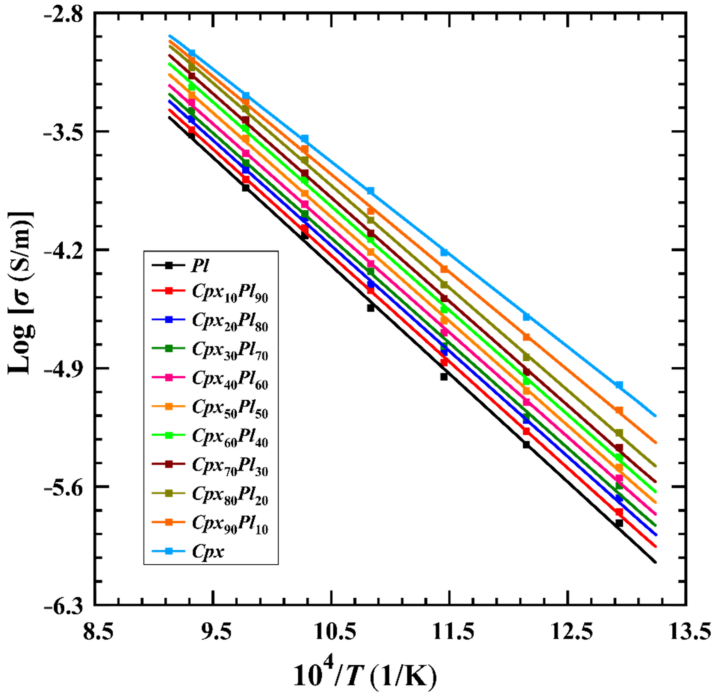

Figure 7. Logarithmic electrical conductivities of dry hot-pressed sintering gabbro with different mineralogical proportions versus reciprocal temperature at temperature ranges of 773–1073 K and 1.0 GPa.

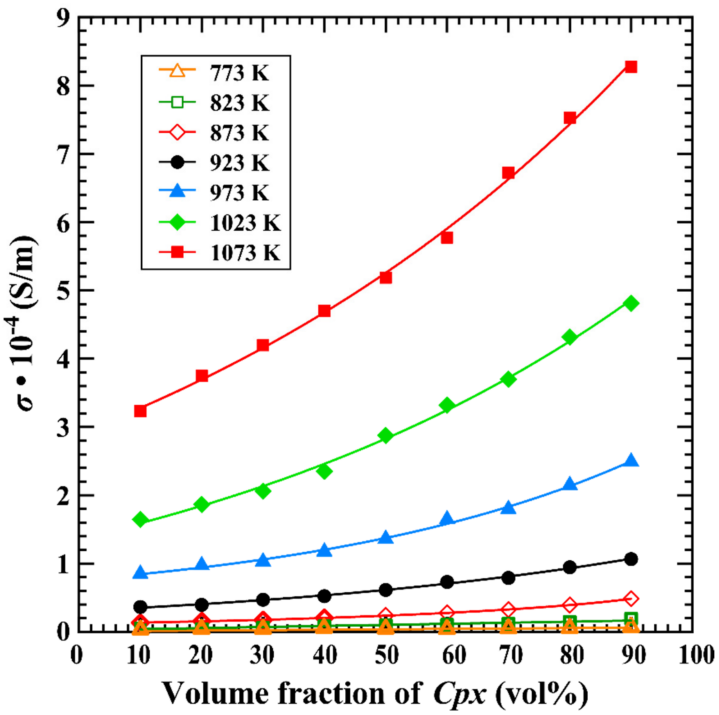

Figure 8. Effect of clinopyroxene content on the electrical conductivity of dry hot-pressed sintering gabbro samples with various mineralogical proportions at temperatures of 773–1073 K and 1.0 GPa.

Figure 7 shows the dependence of the electrical conductivity on temperature for gabbro samples with different mineralogical proportions. With the rise of temperature, the electrical conductivity of each hot-pressed sintering gabbro gradually increases accordingly.

For each correspondent mineralogical proportion (Cpx_XPl_{100-X}, X = 0, 10, 20, 30, 40, 50, 60, 70, 80, 90 and 100 vol%), the logarithm of electrical conductivity of the sample and reciprocal temperature follows a good linear relation, which reveals only one individual conduction mechanism operating the electrical transport process at high pressures.

As for each temperature point, a detailed dependence of the electrical conductivity of hot-pressed sintering gabbro on the volume percentage of clinopyroxene was illustrated in Figure 8. It is clear that the electrical conductivity of hot-pressed sintering gabbro shows a strong dependence on the variation of the volume percentage of clinopyroxene, i.e., electrical conductivity of the sample increases with the rise of the volume percentage of clinopyroxene at a constant temperature condition. At the same mineralogical proportion, the electrical conductivity of dry gabbro gradually increases with the rise of the temperature. Noteworthily, the dependence relation of electrical conductivity of gabbro on the variation of volume percentage of clinopyroxene tends to strengthen when the measured temperature is enhanced from 773 K to 1073 K. As one example at the fixed temperature of 1073 K, when the volume percentage of clinopyroxene is increased from 10% to 90%, the electrical conductivity of hot-pressed sintering gabbro is enhanced from about 3.23×10^{-4} S/m to 8.27×10^{-4} S/m accordingly.

In order to further explore the mineralogical proportion on the electrical conductivity of the hot-pressed sintering gabbro, a function relation for the electrical conductivity of gabbro on the volume percentage of clinopyroxene was established as follows,

$$\sigma = CX_{Cpx}^{\alpha}\exp(-\frac{D+\beta X_{\mathrm{Cpx}}^{\gamma}}{kT}) \quad (4)$$

In here, the pre-exponential factor (σ_0) and activation enthalpy (ΔH) of pressure dependence can be described as the equations of $\sigma_0 = A_0(1 - BP)$ and $\Delta H = D + \beta X_{Cpx}^{\gamma}$, where the C is the pre-exponential factor, the D stands for the activation enthalpy at very small values of X_{Cpx}, X_{Cpx} stands for the volume percentage of clinopyroxene, and all of these parameters including α, β and γ are constants. Therefore, the globally fitting data was adopted to fit it, and the fitting results are shown in Table 4.

Table 4. Fitting parameters of activation enthalpy and pre-exponential factor for the electrical conductivity of dry hot-pressed sintering gabbro with various mineralogical proportions at temperatures of 773–1073 K and 1.0 GPa obtained from $\sigma = CX_{Cpx}^{\alpha}\exp(-\frac{D+\beta X_{Cpx}^{\gamma}}{kT})$. In here, the C stands for the pre-exponential factor, the D stands for the activation enthalpy at very small values of X_{Cpx}, X_{Cpx} stands for the volume percentage of clinopyroxene, and all of these parameters including α, β and γ are constants.

X_{Cpx}	log C	D	α	β	γ
$0.1 \leq X_{Cpx} \leq 0.9$	2.47 ± 1.34	1.25 ± 0.01	0.12 ± 0.05	-8.31 ± 0.91	1.60 ± 0.24

5. Comparisons with Previous Studies

As the dominant endmember of constituent mineral in gabbro, the mineralogical content of clinopyroxene has a significant influence on the electrical conductivity of the sample at conditions of 773–1073 K, 1.0 GPa and controlled oxygen fugacity by a Ni–NiO solid buffer. As displayed in Figure 9a, five previously reported results on the electrical conductivity of natural clinopyroxene were employed to compare it in detail [11–15]. Previous results have already confirmed that the iron content and water content are two crucial influential ingredients in the electrical conductivity of Fe-bearing silicate minerals at high temperatures and high pressures [25,27–30]. In the present studies, some microscopic observations from the electron microprobe and the Fourier transform infrared spectroscopy measurements confirmed that the iron content of clinopyroxene is ~1.62 wt% and belonging to a typically anhydrous sample. The electrical conductivities for our dry clinopyroxene are enhanced from 1.01×10^{-5} S/m to 9.19×10^{-4} S/m as the temperature increases from

773 K to 1073 K at 1.0 GPa. We note that, under the similar experimental conditions, our present results on the electrical conductivity of dry clinopyroxene are in good agreement with the anhydrous clinopyroxene reported by Yang et al. [11] and Zhao and Yoshino [12], but about 1.5 orders of magnitude lower than the electrical conductivities of hydrous sample from Zhao and Yoshino [12]. As noted by Zhao and Yoshino [12], the discrepancies may be due to the differentiation of water content; the electrical conductivities of clinopyroxene can be enhanced by the rise of water content. Liu et al. [14] also carried out the impedance spectroscopic measurements on the omphacite single crystals with their correspondent iron content of 7.92 wt% and the water content of 85 ppm wt at pressure of 1.0 GPa and temperature ranges of 623–973 K. The electrical conductivities for omphacite ($10^{-3.6}$–$10^{-1.3}$ S/m) from Liu et al. [14] are higher than our present acquired results, which is possibly caused by the higher contents of iron and water in their measured omphacite. Our obtained electrical conductivities of clinopyroxene are lower than those of natural diopside with iron content of 4.09 wt%, whereas they are higher than synthetic iron-free diopside from Hinze et al. [13]. All of these discrepancies of the electrical conductivities may originate from the distinction of chemical composition in samples, which resemble the effect of iron content on the electrical conductivity of other main rock-forming silicate minerals at high temperature and high pressure [29]. In addition, electrical conductivities of the clinopyroxene–NaCl–H_2O system were measured at temperature ranges of 673–973 K and 1.0 GPa by Sun et al. [15]. Their electrical conductivities are approximately 4–5 orders of magnitude higher than ours, which can be interpreted as the interconnected NaCl-bearing aqueous fluids, and this can greatly enhance the electrical conductivity of fluid-bearing clinopyroxene at high temperature and high pressure.

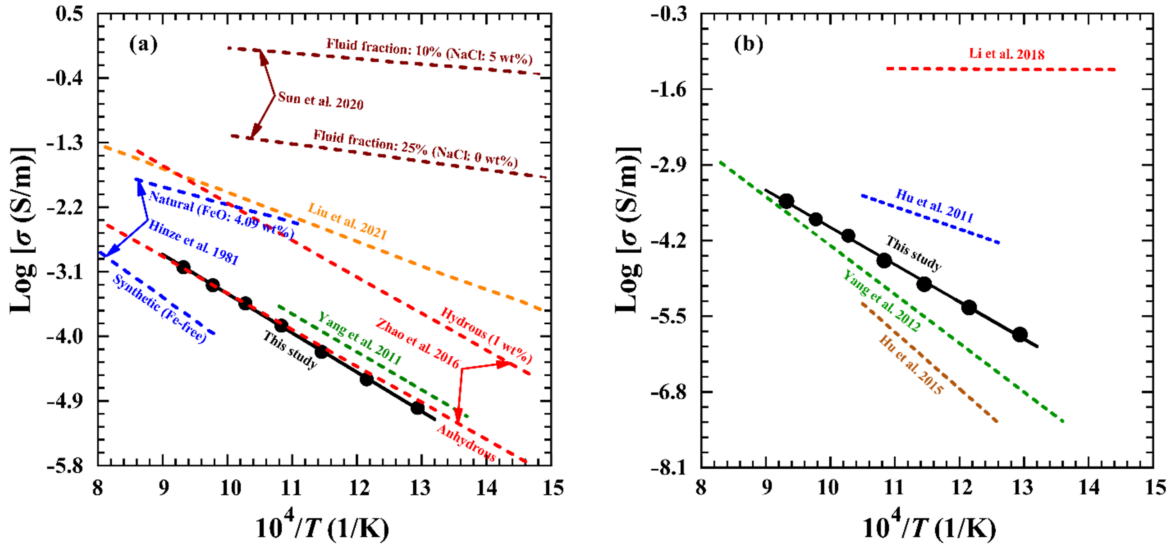

Figure 9. Comparisons of the electrical conductivities of dry clinopyroxene (**a**) and dry plagioclase (**b**) at temperatures of 773–1073 K and 1.0 GPa in present studies with previous results, respectively. The electrical conductivity data for clinopyroxene are from Yang et al. (2011) [11], Zhao et al. (2016) [12] Hinze et al. (1981) [13], Liu et al. (2021) [14] and Sun et al. (2020) [15]. The electrical conductivity data for feldspar are from Yang et al. (2012) [16], Hu et al. (2011, 2015) [17,18], Li et al. (2020) [31].

As another endmember of constituent mineral in gabbro, plagioclase can also alter the chemical composition of hot-pressed sintering samples by changing its corresponding volume percentage, and possibly resulting in the variation of electrical conductivity of gabbro at conditions of high temperature and high pressure. Electrical conductivities of anhydrous plagioclase (its chemical composition is calculated as $An_{57}Ab_{43}$) were investigated under conditions of 773–1073 K and 1.0 GPa, and previously reported results are compared in Figure 9b. It is obvious that our present acquired electrical conductivity

of plagioclase (its chemical composition is calculated as $An_{66}Ab_{32}Or_2$) is higher than the previous results reported by Yang et al. [16]. The dominant charge carrier was extrapolated as the monovalent ion of cationic sodium in dry plagioclase and the electrical conductivity might increase with the rise of cationic sodium concentration. The discrepancy between our results and Yang et al. [16] can be ascribed to the higher content of cationic sodium in our samples. The electrical conductivity of albite reported by Hu et al. [17] was higher than our results of plagioclase at 1.0 GPa, which is possibly related to the distinction in the content of cationic sodium. Although the same dominant charge carriers of cationic sodium between our present plagioclase and previously reported albite from Hu et al. [17] were extrapolated, it is evident that our experimental measured plagioclase contains a relatively lower cationic sodium content. In comparison with Hu et al. [18], the electrical conductivity of anhydrous anorthite is lower than our presently obtained results for plagioclase. As usual, the electrical conductivity of dry feldspar is derived from the ionic diffusion of the charge carrier under a designated electric field of alternating current [32]. According to the previous results on the cationic diffusion reported by Behrens et al. [33], the diffusion coefficient of the monovalent cationic sodium is ~3.7 orders of magnitude higher than the bivalent cationic calcium in the ternary structural feldspars at constant temperature. Due to the Nernst–Einstein equation describing the relation between the electrical conductivity and diffusion coefficient, a relatively higher bivalent calcium ion in Hu et al. [18] can result in abnormally lower electrical conductivity results than ours. Besides, Li et al. [31] measured the electrical conductivities of plagioclase–NaCl–water system at temperatures of 400–900 K and 1.2 GPa. The electrical conductivities of NaCl-bearing fluids in plagioclase increase with the rise of the fluid fraction and salinity, which are close to 2–4.5 orders of magnitude higher than those of our anhydrous plagioclase.

Gabbro, as a representative basic intrusive rock, is mainly composed of clinopyroxene and plagioclase. There are significant differences in the mineralogical proportion of gabbro which are outcropped in different regions of oceanic crust and craton crust [5,6,34,35]. Therefore, electrical conductivities of hot-pressed sintering gabbro with various mineralogical proportions (Cpx_XPl_{100-X}, X = 0, 10, 20, 30, 40, 50, 60, 70, 80, 90 and 100 vol%) were systemically investigated under conditions of temperature ranges from 773 K to 1073 K and 1.0 GPa, which were also compared with the available previously reported results on natural gabbro (Figure 10).

As shown in Figure 10, it is clear that our presently acquired electrical conductivities of dry gabbro with various mineralogical proportions are well consistent with the previously reported results. The electrical conductivities of dry natural gabbro in the Oman ophiolite from Saito and Bagdassarov [10] were performed at conditions of temperature ranges of 523–1181 K and pressures of 0.6–0.8 GPa by using the piston-cylinder high-pressure apparatus. As pointed out by Saito et al. [36], the mineralogical composition of natural Oman gabbro is ~63 vol% of plagioclase, ~18 vol% of clinopyroxene, ~12 vol% of orthopyroxene, ~4 vol% of olivine, ~2 vol% of minor amounts of secondary serpentine, and ~1 vol% of magnetite, and the corresponding chemical composition of plagioclase in natural sample is described as $An_{80}Ab_{20}$. In this study, a series of pure hot-pressed sintering anhydrous gabbro samples with the chemical composition of $An_{57}Ab_{43}$ in plagioclase were selected to investigate the effects of mineralogical proportions on the electrical conductivity of samples at high temperature and high pressure. Some feeble discrepancies in the electrical conductivity results of gabbro between Saito and Bagdassarov [10] and ours are possibly related to the complicated mineralogical composition, the occurrence of the inevitable high-temperature dehydration of secondary serpentine, high conductivity phase of magnetite, and chemical composition of plagioclase ($An_{80}Ab_{20}$). Of course, we also find that the electrical conductivity of dry hot-pressed sintering gabbro is relatively lower, which resembles previously reported results on the electrical conductivity of dry silicate minerals [27–29]. When we compared our presently obtained electrical conductivity results with other natural gabbros with high water content reported by Dai et al. [9] and abnormally high content of

high-conductivity phases reported by Wang et al. [7] and Bai et al. [8], all of these available discrepancies are possibly due to the differentiation in initial sample composition.

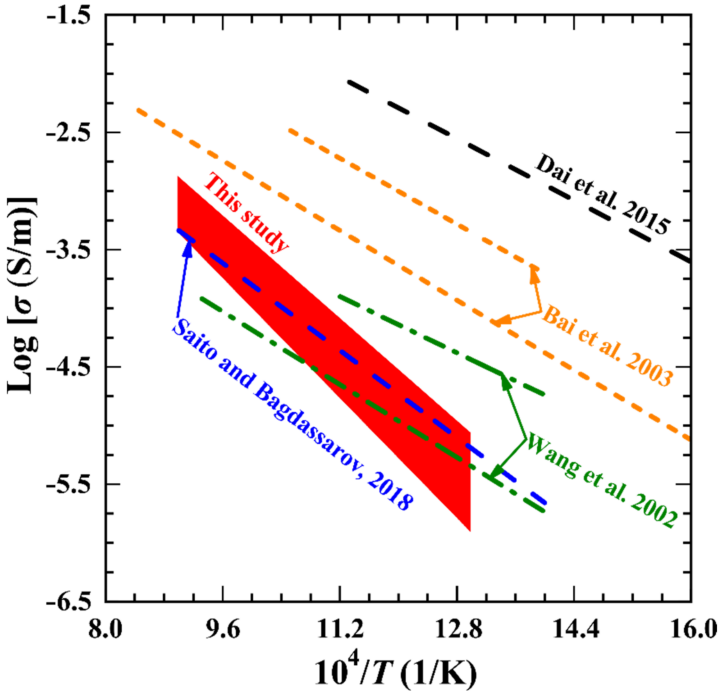

Figure 10. Electrical conductivities of dry hot-pressed sintering gabbro with various mineralogical proportions at the pressure of 1.0 GPa (red shaded area) compared with the previous results.

6. Conduction Mechanism

Since the Arrhenius plot demonstrates a linear relation between the logarithm of electrical conductivity and reciprocal temperature, only one individual conduction mechanism can be identified under various mineralogical compositions (Cpx_XPl_{100-X}, X = 0, 10, 20, 30, 40, 50, 60, 70, 80, 90 and 100 vol%) at the pressure ranges from 1.0 GPa to 3.0 GPa. The present results show that the electrical conductivity of dry hot-pressed gabbro increases with the rise of the volume percentage of clinopyroxene. Previously available reported results demonstrated that the electrical conductivity of dry clinopyroxene depends strongly on iron content and the dominant conduction mechanism is small polaron [11,13,37]. Obviously, the iron content in the hot-pressed sintering gabbro increases with the rise of volume percentage of clinopyroxene, and the electrical conductivities of samples increase with increasing iron content, accordingly. Thus, small polaron is considered to be the dominant conduction mechanism for the anhydrous gabbro. The lattice point defect reactions can be described as follows:

$$Fe^{\times}_{Mg} + h^{\bullet} \rightleftharpoons Fe^{\bullet}_{Mg} \quad (5)$$

where $Fe^{\times}_{Mg}$ and $Fe^{\bullet}_{Mg}$ stand for divalent and trivalent iron ion occupying the site of magnesium ion, and $h^{\bullet}$ stands for a hole, respectively. The main charge carrier of gabbro is the $Fe^{\bullet}_{Mg}$, and it facilitates the conduction by the hopping of the electron between $Fe^{\times}_{Mg}$ and $Fe^{\bullet}_{Mg}$ [9,29,38]. When the nominally anhydrous minerals and rocks contain a trace amount of structural water, it is generally known that some hydrogen-related defects are considered a dominant conduction mechanism [9,27,29]. The FT-IR spectra results indicate that the initial and recovered samples are almost anhydrous. Therefore, the hydrogen-related defects cannot be the dominant conduction mechanism for the anhydrous gabbro. In addition, the ionic conduction is regarded as the main conduction mechanism in some alkali-bearing anhydrous silicate minerals [17,18,39]. It is proposed that the conduction mechanism is the small polaron for dry clinopyroxene and the alkali ion for

dry plagioclase [11,15,16,31]. As shown in Figure 8, the electrical conductivity of the dry hot-pressed sintering gabbro shows a negative dependence relation with increasing the volume percentage of plagioclase, and the contribution of plagioclase to electrical conductivity of gabbro can be ruled out. Consequently, the small polaron might be the dominant conduction mechanism in dry hot-pressed sintering gabbro under conditions of high temperature, high pressure, and various mineralogical compositions.

7. Geophysical Implications

As a typical intrusive rock, gabbro is one of the dominant constituent materials in the regions of oceanic crust and craton crust. Petrological and geochemical evidence have demonstrated that the mineralogical proportions of the main constituent minerals in gabbro show an obvious differentiation in various regions [40,41]. Thus, it is crucial to establish the electrical conductivity–depth profile of dry gabbro with various mineralogical proportions on the base of the regions of oceanic crust and craton crust. The relationship between the temperature and depth in the Earth's stationary crust can be obtained by a numerical solution of the heat conduction equation [42],

$$T = T_0 + \left(\frac{Q}{k}\right) Z - \left(\frac{A_0}{2k}\right) Z^2 \quad (6)$$

where T_0 is the surface temperature (K), Q is the surface heat flow (mW/m^2), Z is the lithosphere layer depth (km), k is thermal conductivity (Wm/K) and A_0 is the lithospheric radiogenic heat productivity (μW/m^3). According to the heat conduction equation and thermal calculation parameters, the electrical conductivity–temperature results can be converted to an electrical conductivity–depth profile [25,43,44]. To simplify the conductivity–depth profile model, some necessary assumptions and extrapolations are proposed as follows: (1) the influence of pressure on the electrical conductivity of anhydrous gabbro is ignored; (2) a Ni–NiO solid buffer is adopted to represent the oxygen fugacity in the regions of oceanic crust and craton crust; (3) in the present studies, the hot-pressed sintering gabbro is anhydrous, the effect of water content on the electrical conductivity of sample does not need to be considered; (4) all of the other potentially influential characteristics, including grain size and grain boundary state, on the electrical conductivity of rock can be neglected; (5) the influence of accessory minerals and high conductive phases on the electrical conductivity of gabbro are ignored; (6) dry hot-pressed sintering gabbro with three typical mineralogical proportions ($Cpx_{10}Pl_{90}$, $Cpx_{50}Pl_{50}$, and $Cpx_{90}Pl_{10}$) are adopted to represent the chemical composition of gabbro-rich regions in the oceanic crust and craton crust.

The electrical conductivity–depth profile based on the electrical conductivity of dry hot-pressed sintering gabbro with three typical mineralogical proportions ($Cpx_{10}Pl_{90}$, $Cpx_{50}Pl_{50,}$ and $Cpx_{90}Pl_{10}$) for the oceanic crust is constructed at depths of 1–7 km (Figure 11a). Concurrently, we also compared with the previous electrical resistivity results reported by Drury [45]. Two representative geothermal gradient values of 30 K/km and 60 K/km are chosen, which are representing the average and relatively steep plutonic sequence in the oceanic crust, respectively [45–47]. From Figure 11a, it is very obvious that the electrical conductivity of hot-pressed sintering dry gabbro at the geothermal gradient of 60 K/km is far higher than that of 30 K/km at each correspondent typical mineralogical proportions ($Cpx_{10}Pl_{90}$, $Cpx_{50}Pl_{50,}$ and $Cpx_{90}Pl_{10}$). At constant geothermal gradients, the electrical conductivity of hot-pressed sintering gabbro will be enhanced ~100 times of magnitude from the $Cpx_{10}Pl_{90}$ to $Cpx_{90}Pl_{10}$ mineralogical proportions. According to the previous results, the electrical conductivity falls within the range of 10^{-4}–10^{-1} S/m in a typical oceanic crust; therefore, the experimental results from the electrical conductivities of the dry hot-pressed sintering gabbro with various mineralogical proportions (Cpx_XPl_{100-X}, X = 0, 10, 20, 30, 40, 50, 60, 70, 80, 90 and 100 vol%) are abnormally lower than the data at depths of 1–7 km.

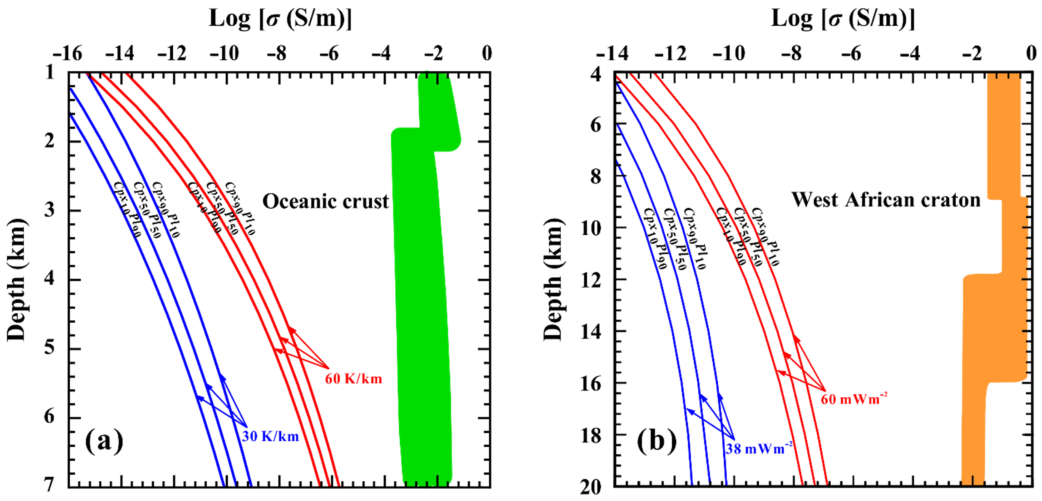

Figure 11. Laboratory-based conductivity–depth profiles constructed from the electrical conductivities of the dry hot-pressed sintering gabbro ($Cpx_{10}Pl_{90}$, $Cpx_{50}Pl_{50,}$ and $Cpx_{90}Pl_{10}$) and the thermodynamic parameters, showing comparison with the conductivity for the anomalous high conductivity zones (HCZ) in the oceanic crust and West African craton, respectively. In (**a**), the red and blue solid lines represent the conductivity–depth profiles on the geothermal gradients of 60 K/km and 30 K/km, respectively. In (**b**), the red solid lines and the blue solid lines are based on the surface heat flow values of 60 mW/m^2 and 38 mW/m^2, respectively. The green region represents the oceanic crust with a high conductivity anomaly in (**a**), and the MT data derived from a high-conductivity anomaly in the West African craton are shown as the orange region in (**b**) (reproduced with permission from the reference of Le Pape et al. [4], published by Elsevier, 2017; reproduced with permission from the reference of Drury [45], published by Oxford University Press, 1979).

At the same time, two typical heat flow values of 38 and 60 mW/m^2 were selected for the West African craton [48,49]. As shown in Figure 11b, the electrical conductivity–depth profile was successfully established from the West African craton at depths of 4–20 km, and the magnetotelluric conductivity results from the West African craton are also included [4]. It is evident that the electrical conductivity of dry hot-pressed sintering gabbro at the heat flow value of 60 mW/m^2 is far higher than that of 38 mW/m^2 at each correspondent typical mineralogical proportions ($Cpx_{10}Pl_{90}$, $Cpx_{50}Pl_{50,}$ and $Cpx_{90}Pl_{10}$). At constant heat flow values, the electrical conductivity of hot-pressed sintering gabbro will be enhanced ~1000 times of magnitude from the $Cpx_{10}Pl_{90}$ to $Cpx_{90}Pl_{10}$ mineralogical proportions. Based on the previous results from the field magnetotelluric data, the electrical conductivities are within the range of 10^{-2}–10^{0} S/m in West African craton. Consequently, the experimental results from the electrical conductivities of the dry hot-pressed sintering gabbro with various mineralogical proportions (Cpx_XPl_{100-X}, X = 0, 10, 20, 30, 40, 50, 60, 70, 80, 90 and 100 vol%) are abnormally lower than field magnetotelluric data at depths of 4–20 km.

In conclusion, our obtained experimental results on the electrical conductivities of the dry hot-pressed sintering gabbro with various mineralogical proportions (Cpx_XPl_{100-X}, X = 0, 10, 20, 30, 40, 50, 60, 70, 80, 90 and 100 vol%) at high temperature and high pressure are abnormally lower than those of field magnetotelluric data of the gabbro-rich regions, which cannot explain the high conductivity anomalies for the oceanic crust and West African craton. Some potential causes need to be considered conscientiously, such as the structural water in nominally anhydrous minerals [9,28,30,50,51], dehydration (oxidation–dehydrogenation) of hydrous minerals [23,52,53], partial melting [54–57], the interconnected high conductive phases [24,28,58,59], and the salinity-bearing (or water-bearing) fluids [15,31,60–62], in the future. Although the present acquired electrical conductivity results on the dry hot-pressed sintering gabbro with various mineralogical proportions cannot explain the high conductivity anomaly in the oceanic crust and West African cra-

ton, it can provide one reasonable constraint on the mineralogical composition in these representative gabbro-rich regions.

Author Contributions: L.D. and H.H.: designing the project; M.W., L.D. and H.H.: writing the initial draft of the work and the final paper, as well as interpreting the results; M.W. and W.S.: performing electrical conductivity experiments; M.W., Z.H. and C.J.: performing and interpreting scanning electron microscope analyses; All authors discussed the results and commented on the manuscript. All authors have read and agreed to the published version of the manuscript.

Funding: This research was financially supported by the NSF of China (42072055, 41774099, 41772042 and 42002043), Youth Innovation Promotion Association of CAS (Grant No.2019390) and Special Fund of the West Light Foundation of CAS (2018).

Data Availability Statement: The data that support the findings of this study are available from the corresponding author upon reasonable request.

Acknowledgments: We thank the editor of Julien Siebert for kindly handling our paper, as well as three anonymous reviewers for their constructive and enlightened advice in the revising process.

Conflicts of Interest: The authors declare no conflict of interest.

References

1. Baba, K. Electrical structure in marine tectonic settings. *Surv. Geophys.* **2005**, *26*, 701–731. [CrossRef]
2. Kaya, T.; Kasaya, T.; Tank, S.B.; Ogawa, Y.; Tuncer, M.K.; Oshiman, N.; Honkura, Y.; Matsushima, M. Electrical characterization of the north anatolian fault zone underneath the Marmara Sea, turkey by ocean bottom magnetotellurics. *Geophys. J. Int.* **2013**, *193*, 664–677. [CrossRef]
3. Usui, Y.; Kasaya, T.; Ogawa, Y.; Iwamoto, H. Marine magnetotelluric inversion with an unstructured tetrahedral mesh. *Geophys. J. Int.* **2018**, *214*, 952–974. [CrossRef]
4. Le Pape, F.; Jones, A.G.; Jessell, M.W.; Perrouty, S.; Gallardo, L.A.; Baratoux, L.; Hogg, C.; Siebenaller, L.; Toure, A.; Ouiya, P.; et al. Crustal structure of southern Burkina Faso inferred from magnetotelluric, gravity and magnetic data. *Precambrian Res.* **2017**, *300*, 261–272. [CrossRef]
5. Ringwood, A.E.; Green, D.H. An experimental investigation of the gabbro-eclogite transformation and some geophysical implications. *Tectonophysics* **1966**, *3*, 383–427. [CrossRef]
6. Christensen, N.I.; Salisbury, M.H. Structure and constitution of the lower oceanic crust. *Rev. Geophys.* **1975**, *13*, 57–86. [CrossRef]
7. Wang, D.J.; Liu, C.Q.; Li, H.P.; Yi, L.; Su, G.L.; Ding, D.Y. Impedance spectra of hot, dry gabbro at high temperature and pressure. *Prog. Nat. Sci.* **2002**, *12*, 397–400.
8. Bai, L.P.; Du, J.G.; Liu, W.; Zhou, W.G. Experimental studies of electrical conductivities and P-wave velocities of gabbro at high pressures and high temperatures. *Sci. China Ser. D* **2003**, *46*, 895–908. [CrossRef]
9. Dai, L.D.; Hu, H.Y.; Li, H.P.; Hui, K.S.; Jiang, J.J.; Li, J.; Sun, W.Q. Electrical conductivity of gabbro: The effects of temperature, pressure and oxygen fugacity. *Eur. J. Mineral.* **2015**, *27*, 215–224. [CrossRef]
10. Saito, S.; Bagdassarov, N.S. Laboratory measurements of electrical conductivity in a gabbro of the Oman ophiolite at high–pressures and high–temperatures: Implications for interpretation of resistivity structures of lower oceanic crust. *J. Miner. Petrol. Sci.* **2018**, *113*, 112–117. [CrossRef]
11. Yang, X.Z.; Keppler, H.; McCammon, C.; Ni, H.W.; Xia, Q.K.; Fan, Q.C. Effect of water on the electrical conductivity of lower crustal clinopyroxene. *J. Geophys. Res. Solid Earth* **2011**, *116*, B04208. [CrossRef]
12. Zhao, C.C.; Yoshino, T. Electrical conductivity of mantle clinopyroxene as a function of water content and its implication on electrical structure of uppermost mantle. *Earth Planet. Sci. Lett.* **2016**, *447*, 1–9. [CrossRef]
13. Hinze, E.; Will, G.; Cemic, L. Electrical conductivity measurements on synthetic olivines and on olivine, enstatite and diopside from Dreiser Weiher, Eifel (Germany) under defined thermodynamic activities as a function of temperature and pressure. *Phys. Earth Planet. Inter.* **1981**, *25*, 245–254. [CrossRef]
14. Liu, H.Y.; Zhang, K.; Ingrin, J.; Yang, X.Z. Electrical conductivity of omphacite and garnet indicates limited deep water recycling by crust subduction. *Earth Planet. Sci. Lett.* **2021**, *559*, 116784. [CrossRef]
15. Sun, W.Q.; Dai, L.D.; Li, H.P.; Hu, H.Y.; Jiang, J.J.; Wang, M.Q. Electrical conductivity of clinopyroxene–NaCl–H_2O system at high temperatures and pressures: Implications for high-conductivity anomalies in the deep crust and subduction zone. *J. Geophys. Res. Solid Earth* **2020**, *125*, e2019JB019093. [CrossRef]
16. Yang, X.Z.; Keppler, H.; McCammon, C.; Ni, H.W. Electrical conductivity of orthopyroxene and plagioclase in the lower crust. *Contrib. Mineral. Petrol.* **2012**, *163*, 33–48. [CrossRef]
17. Hu, H.Y.; Li, H.P.; Dai, L.D.; Shan, S.M.; Zhu, C.M. Electrical conductivity of albite at high temperatures and high pressures. *Am. Mineral.* **2011**, *96*, 1821–1827. [CrossRef]
18. Hu, H.Y.; Dai, L.P.; Li, H.P.; Hui, K.S.; Li, J. Temperature and pressure dependence of electrical conductivity in synthetic anorthite. *Solid State Ionics* **2015**, *276*, 136–141. [CrossRef]

19. Yang, X.Z.; Heidelbach, F. Grain size effect on the electrical conductivity of clinopyroxene. *Contrib. Mineral. Petrol.* **2011**, *163*, 939–947. [CrossRef]
20. Bell, D.R.; Ihinger, P.D.; Rossman, G.R. Quantitative analysis of trace OH in garnet and pyroxenes. *Am. Mineral.* **1995**, *80*, 465–474. [CrossRef]
21. Dai, L.D.; Hu, H.Y.; Li, H.P.; Wu, L.; Hui, K.S.; Jiang, J.J.; Sun, W.Q. Influence of temperature, pressure, and oxygen fugacity on the electrical conductivity of dry eclogite, and geophysical implications. *Geochem. Geophys. Geosyst.* **2016**, *17*, 2394–2407. [CrossRef]
22. Dai, L.D.; Li, H.P.; Hu, H.Y.; Shan, S.M. Experimental study of grain boundary electrical conductivities of dry synthetic peridotite under high-temperature, high-pressure, and different oxygen fugacity conditions. *J. Geophys. Res. Solid Earth* **2008**, *113*, B12211. [CrossRef]
23. Hu, H.Y.; Dai, L.D.; Li, H.P.; Sun, W.Q.; Li, B. Effect of dehydrogenation on the electrical conductivity of Fe-bearing amphibole and its implications for the high conductivity anomalies in subduction zones and continental crust. *Earth Planet. Sci. Lett.* **2018**, *498*, 27–37. [CrossRef]
24. Dai, L.D.; Hu, H.Y.; Sun, W.Q.; Li, H.P.; Liu, C.C.; Wang, M.Q. Influence of high conductive magnetite impurity on the electrical conductivity of dry olivine aggregates at high temperature and high pressure. *Minerals* **2019**, *9*, 44. [CrossRef]
25. Dai, L.D.; Li, H.P.; Hu, H.Y.; Shan, S.M.; Jiang, J.J.; Hui, K.S. The effect of chemical composition and oxygen fugacity on the electrical conductivity of dry and hydrous garnet at high temperatures and pressures. *Contrib. Mineral. Petrol.* **2012**, *163*, 689–700. [CrossRef]
26. Dai, L.D.; Li, H.P.; Hu, H.Y.; Jiang, J.J.; Hui, K.S.; Shan, S.M. Electrical conductivity of $Alm_{82}Py_{15}Grs_3$ almandine-rich garnet determined by impedance spectroscopy at high temperatures and high pressures. *Tectonophysics* **2013**, *608*, 1086–1093. [CrossRef]
27. Dai, L.D.; Karato, S.I. Electrical conductivity of orthopyroxene: Implications for the water content of the asthenosphere. *Proc. Jpn. Acad. B* **2009**, *85*, 466–475. [CrossRef]
28. Dai, L.D.; Karato, S.I. Electrical conductivity of wadsleyite at high temperatures and high pressures. *Earth Planet. Sci. Lett.* **2009**, *287*, 277–283. [CrossRef]
29. Dai, L.D.; Karato, S.I. Influence of FeO and H on the electrical conductivity of olivine. *Phys. Earth Planet. Inter.* **2014**, *237*, 73–79. [CrossRef]
30. Dai, L.D.; Karato, S.I. High and highly anisotropic electrical conductivity of the asthenosphere due to hydrogen diffusion in olivine. *Earth Planet. Sci. Lett.* **2014**, *408*, 79–86. [CrossRef]
31. Li, P.; Guo, X.Z.; Chen, S.B.; Wang, C.; Yang, J.L.; Zhou, X.F. Electrical conductivity of the plagioclase–NaCl–water system and its implication for the high conductivity anomalies in the mid-lower crust of Tibet Plateau. *Contrib. Mineral. Petrol.* **2018**, *173*, 16. [CrossRef]
32. Dai, L.D.; Hu, H.Y.; Li, H.P.; Sun, W.Q.; Jiang, J.J. Influence of anisotropy on the electrical conductivity and diffusion coefficient of dry K-feldspar: Implications for the mechanism of conduction. *Chin. Phys. B* **2018**, *27*, 028703. [CrossRef]
33. Behrens, H.; Johannes, W.; Schmalzried, H. On the mechanisms of cation diffusion processes in ternary feldspars. *Phys. Chem. Minerals* **1990**, *17*, 62–78. [CrossRef]
34. Boudier, F.; Nicolas, A.; Ildefonse, B. Magma chambers in the Oman ophiolite: Fed from the top and the bottom. *Earth Planet. Sci. Lett.* **1996**, *144*, 239–250. [CrossRef]
35. Ilboudo, H.; Sawadogo, S.; Traoré, A.S.; Sama, M.; Wenmenga, U.; Lompo, M. Intrusion-related gold mineralization: Inata gold deposit, Bélahourou district, Northern Burkina Faso (West-Africa). *J. Afr. Earth Sci.* **2018**, *148*, 52–58. [CrossRef]
36. Saito, S.; Ishikawa, M.; Arima, M.; Tatsumi, Y. Laboratory measurements of 'porosity–free' intrinsic *Vp* and *Vs* in an olivine gabbro of the Oman ophiolite: Implication for interpretation of the seismic structure of lower oceanic crust. *Island Arc.* **2015**, *24*, 131–144. [CrossRef]
37. Huebner, J.S.; Voigt, D.E. Electrical conductivity of diopside: Evidence for oxygen vacancies. *Am. Mineral.* **1988**, *73*, 1235–1254.
38. Poe, B.T.; Romano, C.; Varchi, V.; Misiti, V.; Scarlato, P. Electrical conductivity of a phonotephrite from Mt. Vesuvius: The importance of chemical composition on the electrical conductivity of silicate melts. *Chem. Geol.* **2008**, *256*, 193–202. [CrossRef]
39. Hu, H.Y.; Li, H.P.; Dai, L.D.; Shan, S.M.; Zhu, C.M. Electrical conductivity of alkali feldspar solid solutions at high temperatures and high pressures. *Phys. Chem. Minerals* **2013**, *40*, 51–62. [CrossRef]
40. Wiebe, R.A. The pleasant bay layered gabbro-diorite, coastal maine: Ponding and crystallization of basaltic injections into a silicic magma chamber. *J. Petrol.* **1993**, *34*, 461–489. [CrossRef]
41. Khromykh, S.V.; Izokh, A.E.; Gurova, A.V.; Cherdantseva, M.V.; Savinsky, I.A.; Vishnevsky, A.V. Syncollisional gabbro in the Irtysh shear zone, Eastern Kazakhstan: Compositions, geochronology, and geodynamic implications. *Lithos* **2019**, *346–347*, 105144. [CrossRef]
42. Selway, K.; Yi, J.; Karato, S.I. Water content of the Tanzanian lithosphere from magnetotelluric data: Implications for cratonic growth and stability. *Earth Planet. Sci. Lett.* **2014**, *388*, 175–186. [CrossRef]
43. Dai, L.D.; Hu, H.Y.; Li, H.P.; Jiang, J.J.; Hui, K.S. Influence of temperature, pressure, and chemical composition on the electrical conductivity of granite. *Am. Mineral.* **2014**, *99*, 1420–1428. [CrossRef]
44. Sun, W.Q.; Dai, L.D.; Li, H.P.; Hu, H.Y.; Liu, C.C.; Wang, M.Q. Effect of temperature, pressure and chemical compositions on the electrical conductivity of schist: Implications for electrical structures under the Tibetan plateau. *Materials* **2019**, *12*, 961. [CrossRef] [PubMed]

45. Drury, M.J. Electrical resistivity models of the oceanic crust based on laboratory measurements on basalts and gabbros. *Geophys. J. R. Astron. Soc.* **1979**, *56*, 241–253. [CrossRef]
46. Hyndman, R.D.; Drury, M.J. The physical properties of oceanic basement rocks from deep drilling on the mid-Atlantic ridge. *J. Geophys. Res.* **1976**, *81*, 4042–4052. [CrossRef]
47. Nehlig, P.; Juteau, T. Flow porosities, permeabilities and preliminary data on fluid inclusions and fossil thermal gradients in the crustal sequence of the Sumail ophiolite (Oman). *Tectonophysics* **1988**, *151*, 199–221. [CrossRef]
48. Lucazeau, F.; Lesquer, A.; Vasseur, G. *Trends of Heat Flow Density from West Africa. Terrestrial Heat Flow and the Lithosphere Structure. Exploration of the Deep Continental Crust*; Čermák, V., Rybach, L., Eds.; Springer: Berlin, Germany, 1991; pp. 417–425.
49. Le Pape, F.; Jones, A.G.; Jessell, M.W.; Hogg, C.; Siebenaller, L.; Perrouty, S.; Touré, A.; Ouiya, P.; Boren, G. The nature of the southern West African craton lithosphere inferred from its electrical resistivity. *Precambrian Res.* **2021**, *358*, 106190. [CrossRef]
50. Dai, L.D.; Hu, H.Y.; He, Y.; Sun, W.Q. Some new progress in the experimental measurements on electrical property of main minerals in the upper mantle at high temperatures and high pressures. In *Mineralogy*; René, M., Ed.; IntechOpen: London, UK, 2022; *in press*. [CrossRef]
51. Dai, L.D.; Karato, S.I. Electrical conductivity of Ti-bearing hydrous olivine aggregates at high temperature and high pressure. *J. Geophys. Res. Solid Earth* **2020**, *125*, e2020JB020309. [CrossRef]
52. Manthilake, G.; Mookherjee, M.; Bolfan-Casanova, N.; Andrault, D. Electrical conductivity of lawsonite and dehydrating fluids at high pressures and temperatures. *Geophys. Res. Lett.* **2015**, *42*, 7398–7405. [CrossRef]
53. Hu, H.Y.; Dai, L.D.; Li, H.P.; Hui, K.S.; Sun, W.Q. Influence of dehydration on the electrical conductivity of epidote and implications for high conductivity anomalies in subduction zones. *J. Geophys. Res. Solid Earth* **2017**, *122*, 2751–2762. [CrossRef]
54. Maumus, J.; Bagdassarov, N.; Schmeling, H. Electrical conductivity and partial melting of mafic rocks under pressure. *Geochim. Cosmochim. Acta* **2005**, *69*, 4703–4718. [CrossRef]
55. Pommier, A.; Leinenweber, K.; Kohlstedt, D.L.; Qi, C.; Garnero, E.J.; Mackwell, S.J.; Tyburczy, J.A. Experimental constraints on the electrical anisotropy of lithosphere-asthenosphere system. *Nature* **2015**, *522*, 202–206. [CrossRef] [PubMed]
56. Guo, X.; Zhang, L.; Su, X.; Mao, Z.; Gao, X.Y.; Yang, X.Z.; Ni, H.W. Melting inside the Tibetan crust? Constraint from electrical conductivity of peraluminous granitic melt. *Geophys. Res. Lett.* **2018**, *45*, 3906–3913. [CrossRef]
57. Freitas, D.; Manthilake, G.; Chantel, J.; Bouhifd, M.A.; Andrault, D. Simultaneous measurements of electrical conductivity and seismic wave velocity of partially molten geological materials: Effect of evolving melt texture. *Phys. Chem. Minerals* **2019**, *46*, 535–551. [CrossRef]
58. Jödicke, H.; Nover, G.; Kruhl, J.H.; Markfort, R. Electrical properties of a graphite-rich quartzite from a former lower continental crust exposed in the Serre San Bruno, Calabria (southern Italy). *Phys. Earth Planet. Inter.* **2007**, *165*, 56–67. [CrossRef]
59. Sun, W.Q.; Jiang, J.J.; Dai, L.D.; Hu, H.Y.; Wang, M.Q.; Qi, Y.Q.; Li, H.P. Electrical properties of dry polycrystalline olivine mixed with various chromite contents: Implications for the high conductivity anomalies in subduction zones. *Geosci. Front.* **2021**, *12*, 101178. [CrossRef]
60. Huang, Y.; Guo, H.; Nakatani, T.; Uesugi, K.; Nakamura, M.; Keppler, H. Electrical conductivity in texturally equilibrated fluid-bearing forsterite aggregates at 800 °C and 1 GPa: Implications for the high electrical conductivity anomalies in mantle wedges. *J. Geophys. Res. Solid Earth* **2021**, *126*, e2020JB021343. [CrossRef]
61. Hu, H.Y.; Dai, L.D.; Sun, W.Q.; Zhuang, Y.K.; Liu, K.X.; Yang, L.F.; Pu, C.; Hong, M.L.; Wang, M.Q.; Hu, Z.M.; et al. Some remarks on the electrical conductivity of hydrous silicate minerals in the Earth crust, upper mantle and subduction zone at high temperatures and high pressures. *Minerals* **2022**, *12*, 161. [CrossRef]
62. Sun, W.Q.; Jiang, J.J.; Dai, L.D.; Hu, H.Y.; Wang, M.Q.; Qi, Y.Q.; Li, H.P. Influence of saline fluids on the electrical conductivity of olivine aggregates at High temperature and high pressure and its geological implications. *Front. Earth Sci.* **2021**, *9*, 749896. [CrossRef]